Supporting information

Multiplexed optical differentiator enabled by single-size nanostructured metasurface

Xiao Liang[1], Zhou Zhou[1], Zile Li[1,2]*, Jiaxin Li[1], Chang Peng[1], Hao Cui[4], Kai Wei[4], Zhixue He[2], Shaohua Yu[2]* and Guoxing Zheng[1,2,3,5]*

[1]Electronic Information School, Wuhan University, Wuhan, 430072, China

[2]Peng Cheng Laboratory, Shenzhen, 518055, China

[3]Wuhan Institute of Quantum Technology, Wuhan 430206, China

[4]Institute of Optics and Electronics, Chinese Academy of Sciences, Chengdu 610209, China

[5]Hubei Luojia Laboratory, Wuhan 430079, China

Correspondence and requests for materials should be addressed to Z. Li (email: lizile@whu.edu.cn) or to S. Yu (email: yush@cae.cn) or to G. Zheng (email: gxzheng@whu.edu.cn)

Supplementary Note 1: Design principle of order multiplexing differentiator

Supplementary Note 2: Comparison of the 1st- and 2nd-order differentiation results between metasurface output and its ideal counterpart based on a modified method

Supplementary Note 3: Characterization of the fabricated sample 2 used for image edge detection

Supplementary Note 4: Analysis of the broadband response of the 1st-order differentiation and the narrowband response of the 2nd-order differentiation

Supplementary Note 1: Design principle of order multiplexing differentiator

The main idea behind metasurface for 1st- and 2nd-order differentiation is that their transfer function can be readily switched by controlling the polarization state of output light. In order to prove this property, we performed the following analysis.

The Jones matrix of an anisotropic nanostructure with an in-plane orientation angle θ can be expressed as

$$T(\theta) = R(-\theta)T_0R(\theta) = \begin{bmatrix} cos\theta & -sin\theta \\ sin\theta & cos\theta \end{bmatrix} \cdot \begin{bmatrix} A & 0 \\ 0 & D \end{bmatrix} \cdot \begin{bmatrix} cos\theta & sin\theta \\ -sin\theta & cos\theta \end{bmatrix} \tag{S1}$$

where $R(\theta)$ is the rotation matrix, A and D are the complex reflection coefficients along the long and short axes of the nanostructure, respectively.

If the incident light passes through a bulk-optic polarizer, an anisotropic nanostructure and a bulk-optic analyzer sequentially, the Jones vector of output light can be expressed as

$$J = \begin{bmatrix} cos^2\alpha_2 & sin\alpha_2 cos\alpha_2 \\ sin\alpha_2 cos\alpha_2 & sin^2\alpha_2 \end{bmatrix} \cdot T(\theta) \cdot \begin{bmatrix} cos\alpha_1 \\ sin\alpha_1 \end{bmatrix} = \begin{bmatrix} cos^2\alpha_2 & sin\alpha_2 cos\alpha_2 \\ sin\alpha_2 cos\alpha_2 & sin^2\alpha_2 \end{bmatrix} \cdot$$
$$\begin{bmatrix} cos\theta & -sin\theta \\ sin\theta & cos\theta \end{bmatrix} \cdot \begin{bmatrix} A & 0 \\ 0 & D \end{bmatrix} \cdot \begin{bmatrix} cos\theta & sin\theta \\ -sin\theta & cos\theta \end{bmatrix} \cdot \begin{bmatrix} cos\alpha_1 \\ sin\alpha_1 \end{bmatrix}. \tag{S2}$$

We can deduce the complex amplitude of the output light as

$$E = \frac{A-D}{2} cos(2\theta - \alpha_2 - \alpha_1) + \frac{A+D}{2} cos(\alpha_2 - \alpha_1), \tag{S3}$$

where α_1 and α_2 represent the polarization directions of the bulk-optic polarizer and analyzer, respectively.

Specially, if the nanostructure acts as an ideal polarizer (i.e., A = 1 and D = 0), $\alpha_1 = \pi/2$ and $\alpha_2 = 0$, mathematically, under small angle approximation (SAA), we can simplify Eq. S3 as

$$E_{order1} = \frac{1}{2} sin2\theta \sim \theta \tag{S4}$$

Next, if we rotate the transmission axis of the analyzer from 0 to π/2 (i.e., $\alpha_2 = \pi/2$), we can simplify Eq. S3 as

$$E_{order2} = sin^2\theta \sim \theta^2 \tag{S5}$$

Supplementary Fig. 1 shows the amplitude distribution of nanostructures with different orientation angle θ. We can see that at the interval of [-π/8 π/8], the metasurface-based transfer function has good accordance with ideal ones both for the 1st- and 2nd-order differentiation.

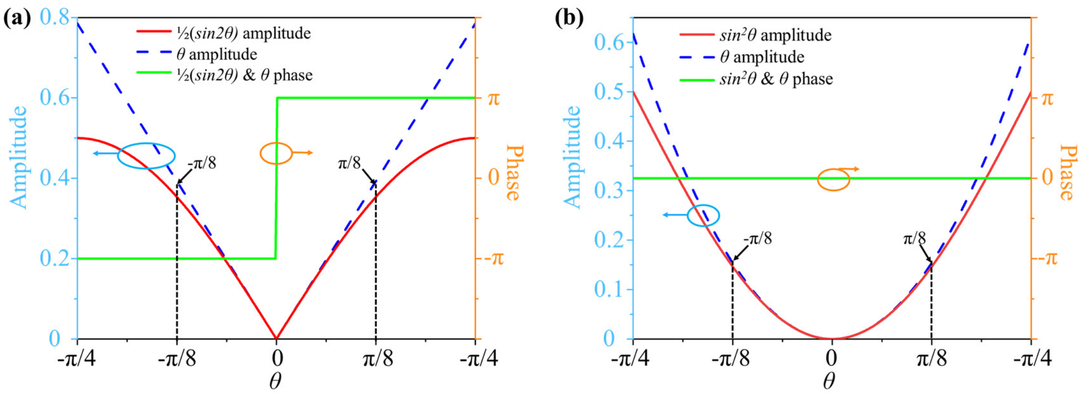

Supplementary Figure 1. The complex amplitude distribution of nanostructures with different orientation angles *θ*. (a, b) Designed by SAA and ideal transfer function of the 1st- and 2nd-order differentiation.

To quantitatively estimate the quality of the metasurface designed by SAA performing the 1st- and 2nd-order differentiation, the correlation coefficients (CC) between the operation results of measurface and the ideal one are analyzed as the criterion. The CC can be express as

$$cc(I,M) = \frac{cov(I,M)}{\sqrt{Var(I)}\sqrt{Var(M)}} \tag{S6}$$

where I and M represent the calculated and ideal one, $cov(I,M)$ is the covariance of I and M, $Var(I)$ and $Var(M)$ represent the variances of I and M, respectively.

Here, taking the angle ranges from –π/8 to π/8 as an example. As shown in Supplementary Fig. 2, it shows the comparison between the calculation results of the 1st- and 2nd-order differentials obtained by different functions under the design scheme of SAA and the ideal results. It is easy to observe that the SAA output is very close to the ideal one.

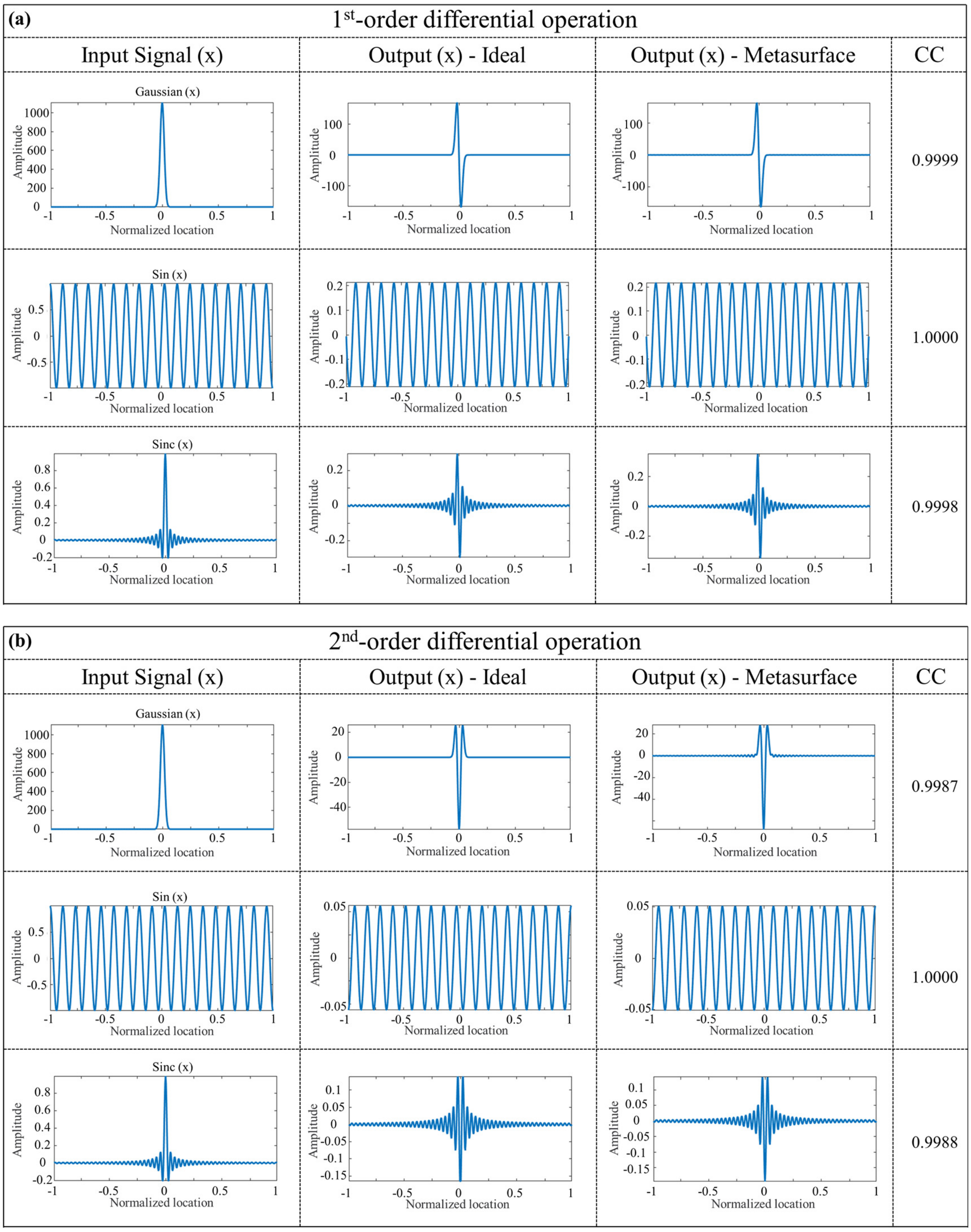

Supplementary Figure 2. The differential result of metasurface designed by SAA. (a) 1st-order differentiation. (b) 2nd-order differentiation. The first, second, third and four columns of (a) and (b) represent the input signal, ideal output, metasurface output and the CC between ideal and metasurface output, respectively.

Supplementary Note 2: Comparison of the 1st- and 2nd-order differentiation results between metasurface output and its ideal counterpart based on a modified method

Considering that 1st-order differentiator is more basic and common in practical application, we chose nanostructures' angle range from -π/4 to π/4 and adopted a modified design to achieve accurate 1st-order differentiation, i.e., the orientation angle θ is designed to ensure that $sin2\theta$ is proportional to ik_x. In this case, 2nd-order differentiation can still be satisfied. The corresponding designed and ideal transfer functions of the 1st- and 2nd-order differentiation are shown in Fig. 3a and 3b, respectively. Here, we introduce the minimum root mean square error (RMSE) to evaluate the error between the 2nd-order differential transfer function of metasurface-based and ideal one, the RMSE can be express as:

$$RMSE = \sqrt{\frac{1}{n}\sum_{i=1}^{n}(sin^2\theta_i - t\theta_i^2)^2} \tag{S7}$$

where n represents the pixel number of samples. $sin^2\theta_i$ and θ_i^2 represent the 2nd-order differential transfer function of metasurface-based and ideal one. t represents the proportional coefficient between $sin^2\theta_i$ and θ_i^2. It is worth noting that t only affects the overall energy of the output signal and does not affect the experimental effect of the 2nd-order differentiation. The RMSE is marked at the top right corner of Fig. 3b.

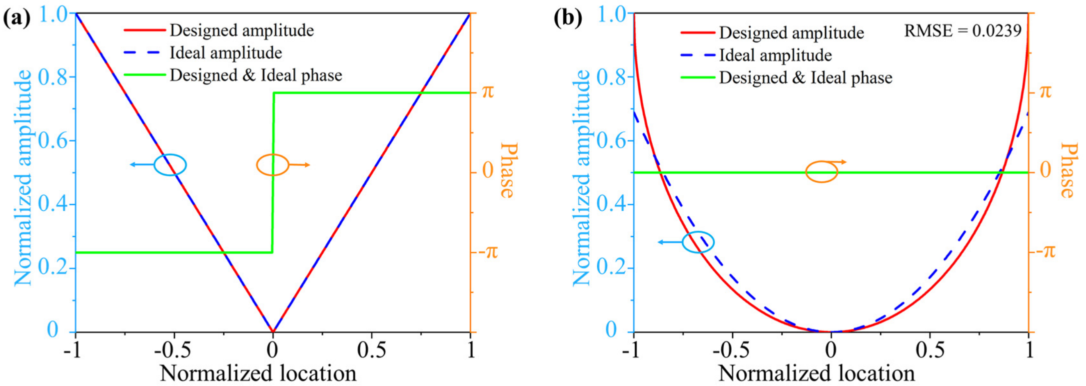

Supplementary Figure 3. Designed and ideal transfer functions of the 1st- and 2nd-order differentiation. (a) 1st-order differentiation. (b) 2nd-order differentiation.

Here taking different functions as examples of the input, we compare the metasurface-based differentiation with its ideal counterpart to evaluate the performance of our design. As shown in Supplementary Fig. 4, it is easy to observe that the metasurface output agrees well with the ideal ones. The expansion of the selected angle range (from [-π/8 π/8] to [-π/4 π/4]) will improve the working efficiency and reduce fabricating difficulty. Therefore, the modified design has the advantages of both high efficiency and simple fabrication.

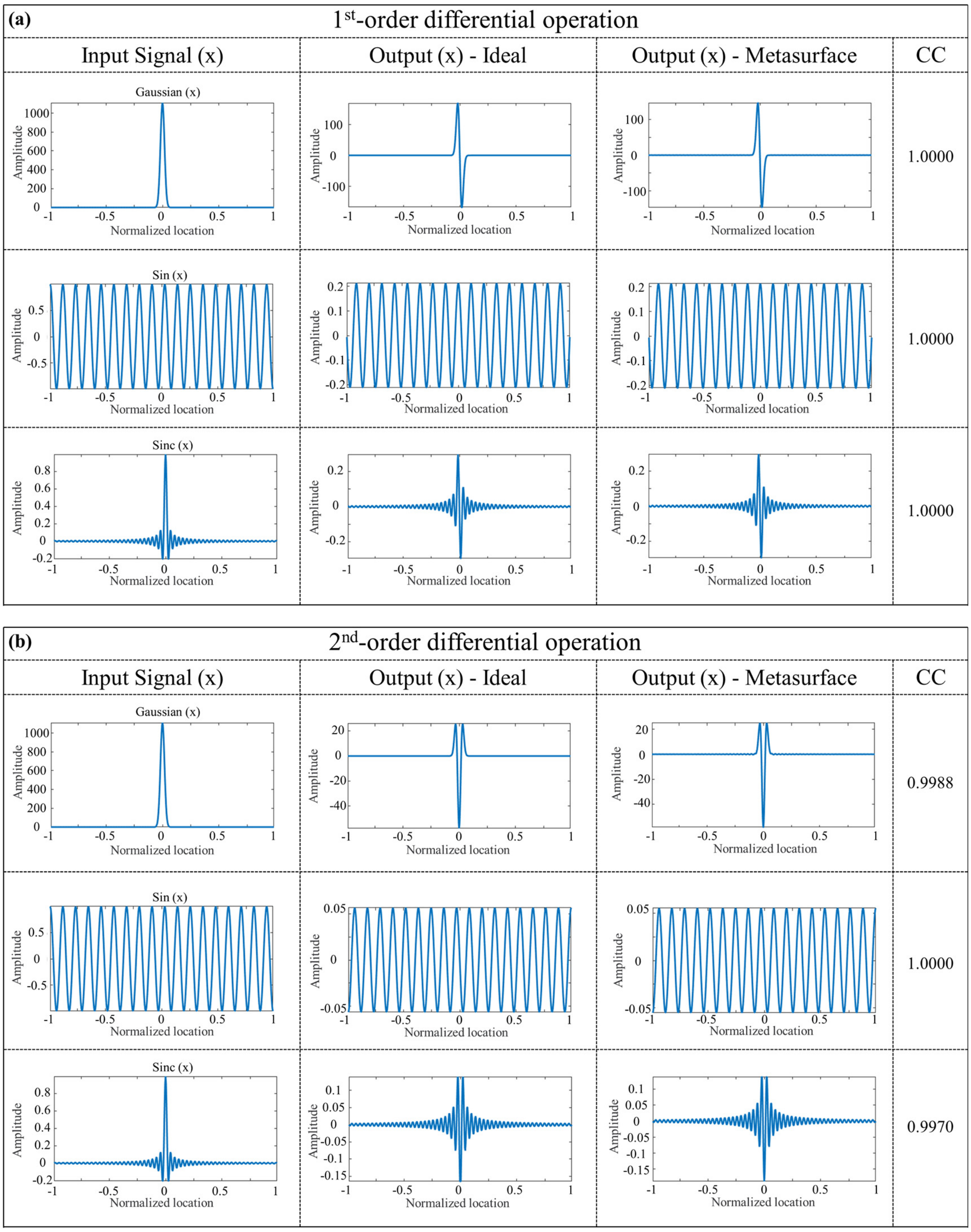

Supplementary Figure 4. The differential result of metasurface designed by a modified method. (a) 1st-order differentiation. (b) 2nd-order differentiation. The first, second, third and four columns of (a) and (b) represent the input signal, ideal output, metasurface output and the CC between ideal and metasurface output, respectively.

Supplementary Note 3: Characterization of the fabricated sample 2 used for image edge detection

In this work, we fabricated two samples (sample 1 with diameters of 150.3 μm for the differential operation of Gaussian beam, sample 2 with diameters of 480.3 μm for detecting the edges of an image), the fabricated sample 2 and the partial SEM image of sample 2 is shown in Supplementary Fig. 5a and 5b, respectively.

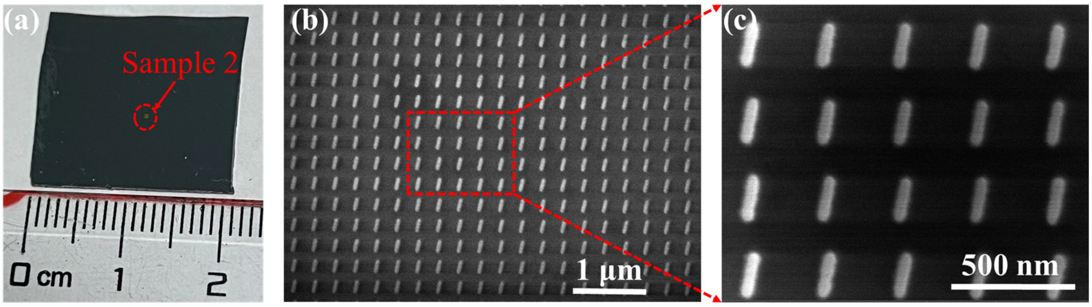

Supplementary Figure 5. (a) Fabricated sample 2. (b) Partial SEM image of sample 2. (c) Zoomed-in view of the red dotted box region in (b).

Supplementary Note 4: Analysis of the broadband response of the 1st-order differentiation and the narrowband response of the 2nd-order differentiation

As shown in Supplementary Fig. 6a and 6c, based on Eq. S3, for the 1st-order differentiation ($\alpha_1 = \pi/2$ and $\alpha_2 = 0$), no matter what the operating wavelength is, the amplitude manipulation of the nanostructures change linearly with position, i.e., $H(k_x) \propto ik_x$. Therefore, the 1st-order differentiation can be achieved with different efficiency. For the 2nd-order differentiation ($\alpha_1 = \pi/2$ and $\alpha_2 = \pi/2$), however, $H(k_x)$ no longer satisfies the positive correlation with $(ik_x)^2$ when the operating wavelength deviates from the operating wavelength, the relationships between the amplitude manipulation obtained from Eq. S3 and the position are shown in Supplementary Fig. 6b and 6d. Hence, the 1st-order differentiation has broadband characteristic and the 2nd-order differentiation has narrowband characteristic.

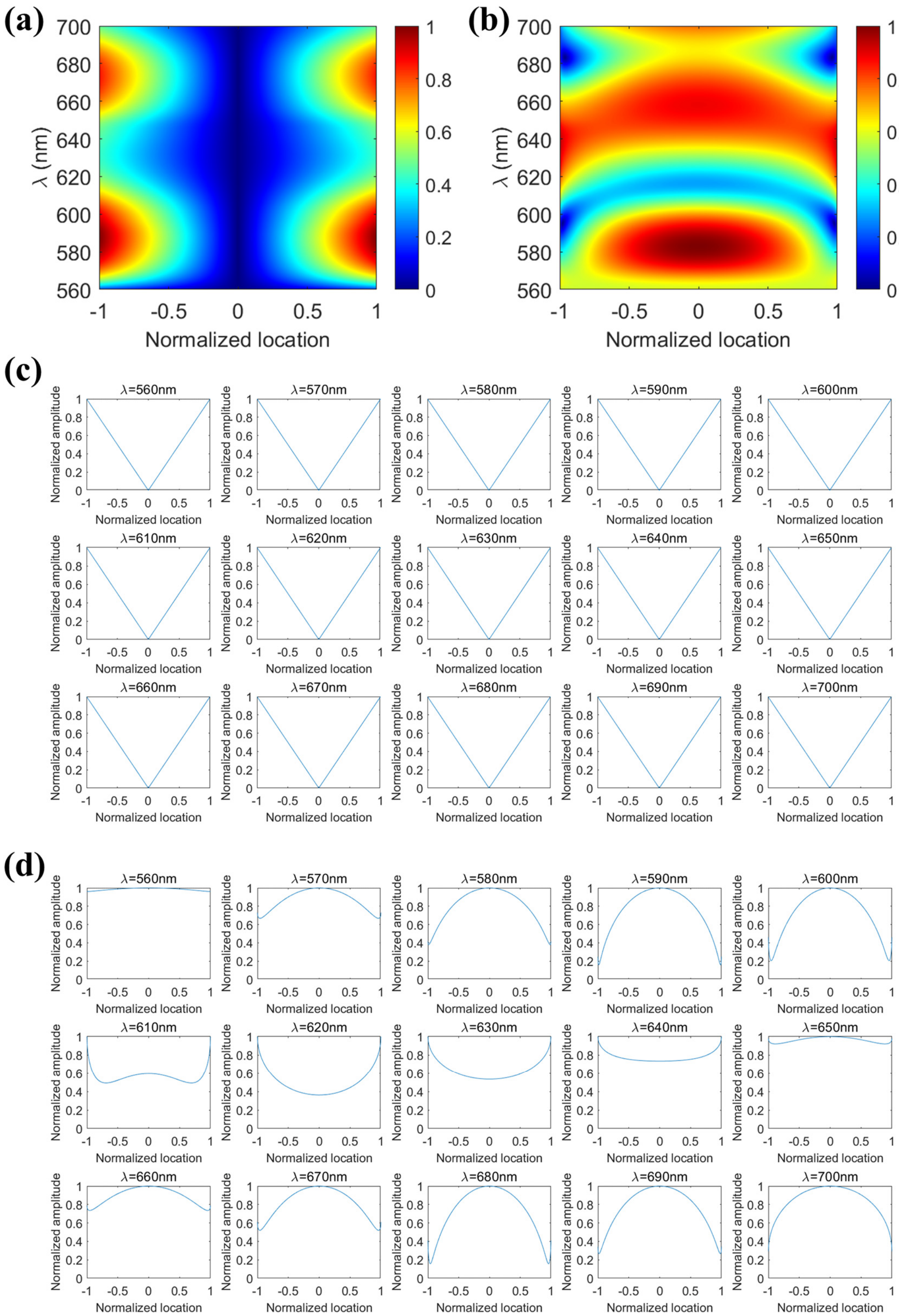

Supplementary Figure 6. The amplitude manipulation of nanostructures with different positions on the metasurface over a wavelength range from 560 nm to 700 nm. (a) 1st-order differentiation. (b) 2nd-order differentiation. (c, d) Plot of the amplitude distribution in (a) and (b) with wavelengths ranging from 560 to 700 nm in steps of 10 nm, respectively.